

Constraints on Cold Magnetized Shocks in Gamma-Ray Bursts

Ramesh Narayan^{1*}, Pawan Kumar^{2*} and Alexander Tchekhovskoy^{3*†}

¹*Harvard-Smithsonian Center for Astrophysics, Harvard University, 60 Garden Street, Cambridge, MA 02138, USA*

²*Astronomy Department, University of Texas, Austin, TX 78712, USA*

³*Princeton Center for Theoretical Science, Jadwin Hall, Princeton University, Princeton, NJ 08544, USA*

Accepted 2011 June 6. Received 2011 April 29

ABSTRACT

We consider a model in which the ultra-relativistic jet in a gamma-ray burst (GRB) is cold and magnetically accelerated. We assume that the energy flux in the outflowing material is partially thermalized via internal shocks or a reverse shock, and we estimate the maximum amount of radiation that could be produced in such magnetized shocks. We compare this estimate with the available observational data on prompt γ -ray emission in GRBs. We find that, even with highly optimistic assumptions, the magnetized jet model is radiatively too inefficient to be consistent with observations. One way out is to assume that much of the magnetic energy in the post-shock, or even pre-shock, jet material is converted to particle thermal energy by some unspecified process, and then radiated. This can increase the radiative efficiency sufficiently to fit observations. Alternatively, jet acceleration may be driven by thermal pressure rather than magnetic fields. In this case, which corresponds to the traditional fireball model, sufficient prompt GRB emission could be produced either from shocks at a large radius or from the jet photosphere closer to the center.

Key words: acceleration of particles – MHD – radiation mechanisms: non-thermal – relativistic processes – shock waves – gamma-ray burst: general

1 INTRODUCTION

A great deal of progress has been made in our understanding of gamma-ray bursts (GRBs), thanks to the launch of a number of dedicated satellites (BeppoSAX, HETE-2, Swift and Integral). These satellites rapidly communicate burst locations to ground-based optical and radio telescopes, which has enabled detailed follow up study of the GRB afterglow emission. It is now known that GRBs produce highly relativistic and beamed jets containing energy $\sim 10^{51}$ erg (see Meszaros 2002; Piran 2005; Zhang 2007; Gehrels, Ramirez-Ruiz & Fox 2009, for extensive reviews of these and other developments). It is also well established that there are two classes of GRBs. One class, called long-GRBs — those lasting for more than a few seconds — is produced when a massive star collapses at the end of its nuclear burning life (see Woosley & Bloom 2006 for a review). For the other class, called short-GRBs — those lasting for less than a few seconds — at least some members are believed to result from mergers of compact stars in binary systems (Gehrels et al. 2009, and references therein).

Despite this impressive progress, several fundamental questions remain unanswered. Foremost among these is the composition of the relativistic jets that power GRBs. We do not know whether GRB jets consist of a normal proton-electron plasma or if they are

dominated by electron-positron pairs. Furthermore, it is uncertain whether the jets are dominated by matter or magnetic fields (Poynting outflow). The related question of how the observed γ -ray radiation is produced is also poorly understood.

A popular model for converting jet energy to particle thermal energy and thereby to radiation is the internal shock model (Narayan et al. 1992; Rees, Meszaros 1994; Sari & Piran 1997). According to this model, the relativistic wind from the central engine of a GRB has a variable Lorentz factor, which leads to collisions between faster and slower moving ejecta. A fraction of the kinetic energy of the jet is converted to thermal energy in these “internal” shocks. A fraction of this thermal energy then goes into electrons and is rapidly radiated away as γ -ray photons via synchrotron and inverse-Compton processes. The internal shock model naturally produces the rapid variability observed in the γ -ray emission of GRBs (Sari & Piran 1997). This is one of its principal virtues.

The internal shock model, however, has a problem, viz., the efficiency ϵ_γ (see eq. 12 for the definition) for converting jet energy to radiation is relatively low (Kumar 1999; Lazzati, Ghisellini & Celotti 1999; Panaitescu, Spada & Meszaros 1999). The efficiency depends on the relative Lorentz factor of the colliding blobs, and also, in the case of magnetized ejecta, on the jet magnetization parameter σ (defined in eq. 2). Since the efficiency ϵ_γ of a GRB can be measured directly from observations of the prompt and afterglow emission, we can constrain the parameters of the internal shock model, notably the magnetization σ of the jet material.

* E-mail: rnarayan@cfa.harvard.edu (RN); pk@astro.as.utexas.edu (PK); atchekho@princeton.edu (AT)

† Princeton Center for Theoretical Science Fellow

Another location where the jet energy may possibly be converted to γ -rays might be the deceleration radius where the jet starts to slow down as a result of its interaction with an external medium. Two shocks are formed in this interaction, one of which, the “forward” shock, heats up the external medium and produces the afterglow emission, and the other, the “reverse” shock, propagates into the GRB jet. The energy released in the reverse shock could be radiated as γ -rays via synchrotron and/or inverse-Compton processes.¹ The efficiency for converting jet energy to γ -rays depends on various parameters, including the σ of the jet material.

Thus, in either the internal shock model or the reverse shock model, the γ -ray efficiency ϵ_γ depends on the magnetization σ of the jet. The present work is motivated by the fact that, under some circumstances, we can independently estimate σ for a GRB jet. This follows from the recent work of Tchekhovskoy, Narayan & McKinney (2010b) who studied the properties of a magnetically accelerated GRB jet. If the jet material is cold, i.e., there is no thermal pressure, and all the acceleration is from electromagnetic forces (Poynting-dominated jet), these authors show that σ can be estimated from the terminal Lorentz factor γ_j and the opening angle θ_j of the jet. Both of the latter quantities can be measured from afterglow data. We thus have an opportunity to check if the values of σ obtained from observations of GRB afterglows are consistent with the γ -ray efficiencies ϵ_γ measured for the same GRBs. Carrying out this test is our goal.

In §2 we write down the standard jump conditions for a magnetized relativistic “perpendicular” shock in which the magnetic field is perpendicular to the flow velocity (or parallel to the shock front). By solving the jump conditions, we calculate the efficiency with which the kinetic energy of a cold relativistic magnetized fluid is converted by the shock to thermal energy. In §3, we calculate the efficiency of the internal shock model and compare it against observations, and in §4, we carry out a similar exercise for the reverse shock model. In both cases, we show that there is an inconsistency between the predictions of the model and measured values of ϵ_γ and σ . We discuss the implications of this result in §5 and suggest possible solutions.

2 RELATIVISTIC PERPENDICULAR SHOCK

2.1 Preliminaries

The problem of interest was discussed in detail by Kennel & Coroniti (1984, hereafter KC84). We follow their methods with a few minor changes. We consider a cold magnetized fluid with a magnetic field strength B_0 in its rest frame. We assume ideal magnetohydrodynamics (MHD) and set the electric field in the rest frame to zero. Transforming to a frame in which the magnetized fluid moves with dimensionless velocity $\beta = v/c$, Lorentz factor $\gamma = 1/\sqrt{1-\beta^2}$, in a direction perpendicular to the magnetic field, the magnetic and electric fields become

$$B = \gamma B_0, \quad E = u B_0 = \frac{u}{\gamma} B, \quad u = \beta \gamma = (\gamma^2 - 1)^{1/2}, \quad (1)$$

where u is the relativistic 4-velocity. The fields B and E in the new frame are parallel and perpendicular, respectively, to B_0 , and each is also perpendicular to the velocity.

¹ It would be very difficult to produce the observed γ -ray variability in the reverse shock model unless there is relativistic turbulence in the shocked fluid (Narayan & Kumar 2009; Lazar, Nakar & Piran 2009).

We define the magnetization parameter σ of the moving fluid as the ratio of the Poynting energy flux to the particle rest energy flux. Thus

$$\sigma = \frac{cEB/4\pi}{n\gamma umc^3} = \frac{B^2/4\pi}{n\gamma^2 mc^2} = \frac{B_0^2/4\pi}{nmc^2}, \quad (2)$$

where n is the particle number density in the fluid rest frame and m is the mass of each particle. In the final expression, the numerator is the rest frame “enthalpy” of the magnetic field, which is equal to $[\Gamma_B/(\Gamma_B - 1)](B_0^2/8\pi)$ (taking the adiabatic index of the magnetic field $\Gamma_B = 2$ for compression transverse to the field), and the denominator is the rest energy density. Since we see that σ depends only on rest frame quantities, it is a relativistic invariant and is frame-independent. KC84 use a slightly different definition of σ where they replace γ^2 in the denominator of the third quantity in equation (2) by γu . As a result, their σ is not truly frame-independent. However, the difference between the two definitions is negligibly small for highly relativistic flows.

2.2 Jump Conditions

We follow KC84, except that we use the definition of σ given in equation (2) and avoid certain approximations. We use subscript u for the gas upstream of the shock and subscript d for the downstream gas. The upstream gas is cold ($P_u = 0$), has a magnetization parameter σ , rest number density n_u , and moves with Lorentz factor γ_u in the frame of the shock. The downstream gas is hot ($P_d \neq 0$) with adiabatic index Γ , has number density n_d , and Lorentz factor γ_d . In the shock frame, the magnetic fields in the two regions, B_u and B_d , are related by

$$B_d = \frac{\gamma_d}{u_d} E_d = \frac{\gamma_d}{u_d} E_u = \frac{\gamma_d u_u}{\gamma_u u_d} B_u, \quad (3)$$

where we have used the fact that the electric field is continuous across the shock.

The upstream and downstream gas enthalpy per particle are, respectively,

$$\mu_u = mc^2, \quad \mu_d = mc^2 \left[1 + \frac{\Gamma}{(\Gamma - 1)} \frac{P_d}{n_d mc^2} \right]. \quad (4)$$

The second term inside the square brackets is a dimensionless number which describes the thermal enthalpy per particle of the shocked gas. It can be written as

$$\frac{\Gamma}{(\Gamma - 1)} \frac{P_d}{n_d mc^2} = h(\theta_d) \theta_d, \quad \theta_d = \frac{P_d}{n_d mc^2} = \frac{kT_d}{mc^2}, \quad h(\theta_d) = \frac{\Gamma}{\Gamma - 1}, \quad (5)$$

where θ_d is the relativistic temperature of the downstream gas. When $\theta_d \ll 1$, the gas is non-relativistic, and we have $\Gamma = 5/3$, $h(\theta_d) = 5/2$, whereas when $\theta_d \gg 1$, the gas is ultra-relativistic, and we have $\Gamma = 4/3$, $h(\theta_d) = 4$. At intermediate temperatures ($\theta_d \sim 1$), $h(\theta_d)$ can be written in terms of modified Bessel functions (see Chandrasekhar 1960). For simplicity, we use the following approximation (Service 1986),

$$h(\theta) = \frac{10 + 20\theta}{4 + 5\theta}, \quad (6)$$

which is sufficiently accurate for our purposes. In principle, if the jet material consists of a normal electron-proton plasma, we should allow for two species of particles in the shocked gas, each with a different temperature. We ignore this complication for simplicity.

We have three jump conditions across the shock, corresponding to three fundamental conservation laws. First, mass conservation implies that the mass fluxes on the two sides of the shock must be equal, i.e.,

$$n_u u_u = n_d u_d. \quad (7)$$

Energy conservation requires the energy fluxes to be equal, i.e.,

$$n_u u_u \gamma_u \mu_u + \frac{EB_u}{4\pi} = n_d u_d \gamma_d \mu_d + \frac{EB_d}{4\pi}. \quad (8)$$

Finally, momentum conservation gives the condition

$$n_u u_u^2 \mu_u + \frac{(B_u^2 + E_u^2)}{8\pi} = n_d u_d^2 \mu_d + P_d + \frac{(B_d^2 + E_d^2)}{8\pi}. \quad (9)$$

In the last equation, the terms involving the electric field cancel since $E_u = E_d$. Eliminating μ_d between equations (8) and (9) and simplifying, we obtain the following expression for θ_d :

$$\theta_d = \left[u_d^2 \left(\frac{u_u}{u_d} - \frac{\gamma_u}{\gamma_d} \right) (1 + \sigma) + \left(\frac{\gamma_u^2 u_d}{2u_u} - \frac{\gamma_d^2 u_u}{2u_d} \right) \sigma \right]. \quad (10)$$

In addition, equation (8) can be rewritten in the following simplified form,

$$1 + h(\theta_d)\theta_d = \frac{\gamma_u}{\gamma_d}(1 + \sigma) - \frac{u_u}{u_d}\sigma. \quad (11)$$

Given the upstream quantities u_u and σ , it is straightforward to solve equations (10) and (11) numerically. We guess a value for the downstream velocity u_d and calculate θ_d using equation (10). We then compute $h(\theta_d)$ using the approximation (6) and check whether the condition (11) is satisfied. If it is not, we numerically adjust u_d until the condition is satisfied. We then have the complete solution for all downstream quantities: γ_d , u_d , n_d/n_u , θ_d , μ_d/mc^2 , B_d/B_u .

The results presented in the following sections use the above numerical approach to solve the jump conditions. An alternate approach is to make suitable approximations and obtain analytical solutions of the jump conditions. Appendix A presents analytical solutions corresponding to a number of useful limits.

3 INTERNAL SHOCK MODEL

3.1 Solving the Jump Conditions

We consider two identical blobs, each with magnetization σ , approaching each other and colliding. In the center of mass frame, the blobs have Lorentz factors γ and relativistic velocities $u = \pm \sqrt{\gamma^2 - 1}$. As a result of the collision, two identical shocks move (in opposite directions) into the two blobs.

For given values of γ and σ , we solve the jump conditions numerically and calculate all quantities of interest in the shocked gas. We begin by assuming a value for the upstream Lorentz factor γ_u in the frame of one of the shocks. Following the procedure described in §2.2, we solve for the downstream Lorentz factor γ_d . From γ_u and γ_d , we calculate the relative Lorentz factor γ_{ud} between the two regions (relativistic velocity subtraction) and check whether it corresponds to the desired value of γ . If not, we adjust γ_u until we obtain $\gamma_{ud} = \gamma$. We then have the solution.

Having obtained the solution, we switch to the rest frame of the shocked gas. We assume that a fraction ϵ_e of the thermal enthalpy of the shocked gas W_{gas} goes into electrons and that it is entirely radiated in γ -rays². This gives the energy E_γ that goes into

² This is perhaps a little optimistic. It is possible that only the gas internal energy is radiated, which is $1/\Gamma$ times the enthalpy.

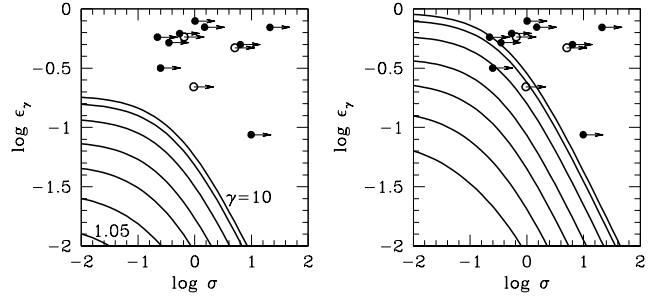


Figure 1. Left: γ -ray efficiency ϵ_γ vs the upstream magnetization parameter σ for an internal shock between two identical blobs. It is assumed that a fraction $\epsilon_e = 0.2$ of the enthalpy in the shocked gas is radiated as prompt γ -rays. From below, the curves correspond to blob Lorentz factor in the center-of-mass frame of $\gamma = 1.05, 1.1, 1.2, 1.4, 2, 4, 10$, respectively. Equivalently, the inter-blob Lorentz factor between the two blobs is $\gamma_{\text{ib}} = 1.21, 1.42, 1.88, 2.92, 7, 31, 199$, respectively. The symbols refer to observational data. The filled circles correspond to the first nine GRBs in Table 1 (PK02 sample) and the open circles to the last three GRBs. The arrows on the symbols indicate that the estimated values of σ are lower limits (eq. 18). Right: Corresponding results for the case when $\epsilon_e = 1$, i.e., all the thermal enthalpy in the shocked gas comes out in prompt γ -rays.

γ -rays. The remaining unradiated enthalpy, which consists of rest mass enthalpy W_{rest} , remaining gas thermal enthalpy $(1 - \epsilon_e)W_{\text{gas}}$ and magnetic enthalpy W_B , contributes to the kinetic energy E_0 that goes into the afterglow. Thus, we estimate the efficiency ϵ_γ of γ -ray emission, the fraction of the total energy that goes into γ -rays, to be

$$\epsilon_\gamma \equiv \frac{E_\gamma}{E_\gamma + E_0} = \frac{\epsilon_e W_{\text{gas}}}{W_{\text{gas}} + W_{\text{rest}} + W_B}. \quad (12)$$

The quantities W_{gas} and W_{rest} are easily obtained from the shock solution. Per particle, they are given by

$$W_{\text{gas}} = h(\theta_d)\theta_d mc^2, \quad W_{\text{rest}} = mc^2. \quad (13)$$

To calculate W_B , we first need to calculate the magnetic field of the shocked gas in the center of mass (CM) frame of the colliding blobs. This is given by

$$B_{\text{CM}} = \frac{B_d}{\gamma_d} = \frac{u_u}{\gamma_u u_d} B_u. \quad (14)$$

Then the magnetic enthalpy per particle is

$$W_B = \frac{B_{\text{CM}}^2}{4\pi n_d} = \frac{u_u}{u_d} \sigma mc^2. \quad (15)$$

Thus we obtain

$$\epsilon_\gamma = \frac{\epsilon_e h(\theta_d)\theta_d}{1 + h(\theta_d)\theta_d + (u_u/u_d)\sigma}. \quad (16)$$

Although all quantities have been estimated in the rest frame of the shocked gas, it is easily shown that Lorentz transforming to a different frame, e.g., the observer frame, will leave ϵ_γ unchanged.

For a given value of ϵ_e , the γ -ray efficiency depends on two parameters, the magnetization σ of the blobs and their Lorentz factor γ in the center-of-mass frame. Figure 1 shows how ϵ_γ varies as a function of σ for selected values of γ , as listed in the figure caption. Instead of γ , we could express the results in terms of the relative inter-blob Lorentz factor of the blobs γ_{ib} . The values of γ_{ib} are also given in the figure caption.

Figure 1 indicates that the maximum radiative efficiency is obtained for unmagnetized blobs. As the magnetization increases, the

amount of thermal energy generated in the shock decreases, reducing the radiative efficiency. This result was already discussed by KC84. The analytical approximations in Appendix A give further details. From §A3 we see that, for $\sigma \ll 1$, the enthalpy of the shocked gas (which is proportional to θ_j) varies as $1 - (5/2)\sigma$, i.e., it reduces with increasing magnetization. The reduction is quite pronounced once $\sigma > 1$; for $\sigma \gg 1$, the enthalpy scales as $1/\sigma$ (§A1).

Note, however, that there is always a shock solution for any choice of γ and σ . This may appear a little surprising since, as we show in Appendix A, a magnetized shock is possible only if the upstream velocity u_u exceeds $\sqrt{\sigma}$. Thus, for strongly magnetized blobs moving in the center-of-mass frame with relatively low velocities, one might think there should be no shock. For example, for $\gamma = 10$ or $u = 9.95$, one might expect the shock to disappear once $\sigma > 3.15$, whereas Fig. 1 shows results for σ values much above this limit.

The explanation is simple. What is relevant for the existence or otherwise of a shock is the upstream velocity in the *shock frame*, not the center-of-mass frame. In all our solutions, the shock moves outward in the center-of-mass frame. When $u^2 \gg \sigma$, the shock velocity is not very large. However, once σ exceeds u^2 , the shock moves quite rapidly into the blob. In fact, it moves so rapidly that the velocity of the upstream gas u_u as seen in the shock frame becomes larger than $\sqrt{\sigma}$, thus permitting a shock. Shocks in this regime are however weak (see §A2), and their radiative efficiencies ϵ_γ are correspondingly very low. As an example, note in Fig. 1 the very low efficiency of the $\gamma = 10$ model (the uppermost curves in the two panels) when $\sigma = 10$.

3.2 Comparison with GRB Data

The data we use are listed in Table 1. Panaitescu & Kumar (2002, hereafter PK02) have analyzed afterglow observations of ten GRBs, and have derived for these objects the parameters we need. We make use of the results in Tables 2 and 3 of their paper. We include GRB 970508 for which we take E_γ from Bloom, Frail & Kulkarni (2003), but we omit GRB 980159 since the redshift is not known. For the remaining 8 systems, we take PK02's estimates of E_γ , the beaming-corrected γ -ray emission in the 20–2000keV band, and E_0 , the beaming-corrected kinetic energy of the afterglow, and compute the γ -ray efficiency parameter ϵ_γ . The afterglow data considered by PK02 did not include observations during the early stages of the afterglow (first day or so). During this time, the external shock is expected to be somewhat radiative. It is thus possible that PK02 slightly underestimated E_0 in their models. To allow for this, we double their values of E_0 and estimate the γ -ray efficiency by $\epsilon_\gamma \sim E_\gamma / (E_\gamma + 2E_0)$. (The correction factor of 2 is probably too large, but our aim is to be conservative.)

In addition, we also estimate the magnetization σ of the jet ejecta. Based on numerical and analytical work on cold magnetically-accelerated GRB jets, Tchekhovskoy et al. (2010b) have shown that the following inequality must be satisfied,

$$\gamma_j \sin \theta_j \lesssim 15\sigma^{1/2}, \quad (17)$$

where γ_j and θ_j are the Lorentz factor and opening angle of the jet ejecta at the conclusion of the prompt emission phase, i.e., just before the onset of the afterglow phase. The factor of 15 is a logarithmic term. Since PK02 have estimated γ_j and θ_j for the 9 GRBs of interest to us (see Table 1), from their data we obtain for each GRB a lower limit on σ ,

$$\sigma_{\min} = \left(\frac{\gamma_j \sin \theta_j}{15} \right)^2. \quad (18)$$

The solid circles in Fig. 1 show the values of σ_{\min} and ϵ_γ for the nine GRBs from the PK02 sample.

In addition, we have gone through the literature and estimated ϵ_γ and σ_{\min} for three more bursts: GRB 021004 (relevant data taken from Bloom, Frail & Kulkarni 2003; Li & Chevalier 2003), GRB 080916C (Abdo et al. 2009; Greiner et al. 2009; Kumar & Barniol Duran 2009), GRB 090510 (Ackermann et al. 2010; Kumar & Barniol Duran 2010). These three GRBs are shown in Fig. 1 with open circles, and the corresponding data are given in the last three lines of Table 1.

In order to compare the data with the predictions of our internal shock model, we need to assume a value for the electron heating parameter ϵ_e . From modeling afterglow observations it is possible to estimate ϵ_e for the forward shock in individual GRBs (e.g., Panaitescu & Kumar 2002). The median value from a sample of 39 GRB afterglows is $\epsilon_e \approx 0.2$ (Santana & Barniol Duran, in preparation). The theoretical curves in the left panel of Fig. 1 correspond to this value of ϵ_e . A quick look shows that the model completely misses the observations for all twelve GRBs in our sample. It has been known for some time that internal shocks involving unmagnetized shocks cannot easily achieve the γ -ray efficiencies required by observations (Kumar 1999; Lazzati, Ghisellini & Celotti 1999; Panaitescu, Spada & Meszaros 1999). Magnetization makes the problem worse. For the σ values estimated for GRBs, the predicted efficiency is much lower than for the unmagnetized case, so the discrepancy is quite large. Note further that the values of σ plotted for the individual GRBs correspond to σ_{\min} (eq. 18). This means that the points might actually lie even farther to the right, which would make the discrepancy impossibly large.

The panel on the right in Fig. 1 shows the highly optimistic case when $\epsilon_e = 1$. This might correspond, for example, to an electron-positron jet. Even in this case, the majority of GRBs are inconsistent with the magnetized internal shock model. We thus conclude that, if jet ejections are magnetized and are described by ideal MHD, and if the blob Lorentz factors γ and γ_{ib} are not very different from the values considered in Fig. 1 (note that the largest value considered is $\gamma_{\text{ib}} \sim 200$ which is very unlikely to be exceeded), then the magnetized internal shock model is ruled out conclusively by the data.

4 REVERSE SHOCK MODEL

4.1 Solving the Jump Conditions

In the case of the reverse shock, we have to consider four regions, as described in Sari & Piran (1995, hereafter SP95):

1. The external unshocked ISM, which is at rest in the lab frame
2. The shocked ISM
3. The shocked jet ejecta
4. The unshocked jet ejecta

Following SP95, we use subscripts 1, 2, 3, 4 to identify quantities in the four regions. Regions 2 and 3 are in pressure equilibrium across the contact discontinuity and move with the same Lorentz factor. As measured in the lab frame, region 1 is at rest, regions 2 and 3 move with Lorentz factor γ_c (c for contact), and region 4 moves with the jet Lorentz factor γ_j .

In the analysis below we consider several distinct frames. First, we have the lab frame in which the unshocked jet moves with Lorentz factor γ_j and the shocked gas moves with γ_c . Next, we have the frame of the forward shock in which the unshocked and shocked ISM move with Lorentz factors γ_1 and γ_2 . Then, we have the frame

Table 1. GRB data (see §3.2 for details).

Source	E_γ^a	E_0^b	ϵ_γ^c	γ_j	$\theta_j(^{\circ})$	σ_{\min}	Ref.
GRB 970508	3.8	20.	0.087	150	18.3	9.86	1,2
GRB 990123	4.9	1.5	0.62	300	2.1	0.54	1
GRB 990510	1.3	1.4	0.32	140	3.1	0.25	1
GRB 991208	18	2.4	0.79	68	12.8	1.01	1
GRB 991216	3.0	1.1	0.58	150	2.7	0.22	1
GRB 000301c	6.6	3.3	0.50	160	13.7	6.38	1
GRB 000418	148	32	0.70	90	50.0	21.1	1
GRB 000926	15	3.2	0.70	130	8.1	1.49	1
GRB 010222	11	5.1	0.52	110	4.6	0.35	1
GRB 021004	560	400	0.58	55	12.7	0.65	2,3
GRB 080916C	8.8×10^4	10^5	0.47	> 880	> 2.2	> 5.07	4,5,6
GRB 090510	1100	4000	0.22	> 1200	0.7	> 0.96	7,8

^a Beaming-corrected energy in γ -rays in units of 10^{50} erg

^b Beaming-corrected kinetic energy in the afterglow in units of 10^{50} erg

^c Calculated using eq. (12) for the last three GRBs, but with E_0 replaced by $2E_0$ for the first nine GRBs

References: 1 – PK02; 2 – Bloom, Frail & Kulkarni (2003); 3 – Li & Chevalier (2003); 4 – Abdo et al. (2009); 5 – Greiner et al. (2009); 6 – Kumar & Barniol Duran (2009); 7 – Ackermann et al. (2010); 8 – Kumar & Barniol Duran (2010).

of the reverse shock in which the unshocked and shocked jet ejecta move with Lorentz factors γ_4 and γ_3 . Finally, we have the frame of the shocked gas. This frame moves with respect to the lab frame with a Lorentz factor γ_c , with respect to the forward shock frame with a relative Lorentz factor γ_2 , and with respect to the reverse shock frame with a relative Lorentz factor γ_3 .

We consider regions 1 and 2 to be essentially unmagnetized and treat the forward shock between these two regions as a hydrodynamic shock. Furthermore, we assume that the relative Lorentz factor across this shock is large, i.e., $\gamma_c, u_c \gg 1$. Let us transform into the frame of the forward shock. The upstream gas is cold ($P_1 = 0$, recall that subscript 1 refers to region 1), is unmagnetized (by assumption, $\sigma = 0$) and has a large Lorentz factor ($\gamma_1 \gg 1$). We can use the results given in §A3 (with subscripts u, d replaced by 1 and 2) in the limit $\sigma \rightarrow 0$ to calculate the properties of the shocked gas. We then obtain the following standard results for the downstream gas,

$$\beta_2 = \frac{1}{3}, \quad \gamma_2 = \frac{3}{2\sqrt{2}}, \quad n_2 = 2\sqrt{2}n_1\gamma_1, \quad P_2 = \frac{2}{3}\gamma_1^2 n_1 mc^2. \quad (19)$$

The relative Lorentz factor between the two regions, which we call γ_c , is equal to $\gamma_1/\sqrt{2}$. Thus, we find

$$n_2 = 4\gamma_c n_1, \quad P_2 = \frac{4}{3}\gamma_c^2 n_1 mc^2. \quad (20)$$

Consider now the reverse shock between the magnetized regions 4 and 3. The jet ejecta have a Lorentz factor γ_j in the lab frame and a magnetization σ . In the frame of the reverse shock, we do not know a priori the value of the upstream Lorentz factor γ_4 . Therefore, as in §3, we will solve for γ_4 via the jump conditions (all the relations given in §2 are valid, except that subscripts u and d should be replaced by 4 and 3, respectively), plus an additional requirement. In §3, the additional constraint was the value of γ (or equivalently γ_{ib}). Here, for easy comparison with previous work in the literature, we will fit a target value of the ‘‘relativity’’ parameter ξ defined in SP95 and Giannios et al. (2008). This parameter is less than unity for a relativistic shock and greater than unity for a Newtonian shock. In Appendix B we show that for a magnetized flow

$$\xi = \left(\frac{R_{\text{dec}}}{R_s} \right)^{1/2} = \left[\frac{3}{\gamma_j^2} \frac{n_4}{n_1} (1 + \sigma) \right]^{1/2}, \quad (21)$$

where R_{dec} and R_s are the deceleration radius and the spreading radius of the expanding ejecta.

Given the jet Lorentz factor γ_j in the lab frame, the magnetization of the jet material σ , and a target value of the relativity parameter ξ , the calculation proceeds as follows. We begin by guessing a value for γ_4 , the Lorentz factor of the upstream jet ejecta as viewed in the frame of the reverse shock. Then, as described in §2, we solve for all quantities in the downstream region 3. In the rest frame of the shocked gas, the gas pressure is equal to

$$P_{3,\text{gas}} = n_3 \theta_3 mc^2 = n_4 \frac{u_4}{u_3} \theta_3 mc^2, \quad (22)$$

and the magnetic pressure is equal to

$$P_{3,\text{mag}} = \frac{B_{3,\text{rest}}^2}{8\pi} = \frac{u_4^2}{\gamma_4^2 u_3^2} \frac{B_4^2}{8\pi} = n_4 \frac{u_4^2}{2u_3^2} \sigma mc^2. \quad (23)$$

Since regions 2 and 3 are in pressure balance, we thus obtain the following condition,

$$P_{3,\text{tot}} = n_4 \left(\frac{u_4}{u_3} \theta_3 + \frac{u_4^2}{2u_3^2} \sigma \right) mc^2 = P_2 = \frac{4}{3} \gamma_c^2 n_1 mc^2. \quad (24)$$

The Lorentz factor γ_c on the right-hand side of equation (24) is straightforward to calculate. In the reverse shock frame, we know that region 4 has a Lorentz factor γ_4 , whereas its Lorentz factor in the lab frame is γ_j (which is given). Thus, we can calculate the Lorentz factor of the reverse shock as seen in the lab frame (relativistic velocity subtraction). Once we have this quantity, we can transform γ_3 (which is in the reverse shock frame) to the lab frame to obtain γ_c , the Lorentz factor of region 3 (as well as region 2) in the lab frame.

Having calculated γ_c , we obtain the density ratio n_4/n_1 from equation (24), and hence the value of ξ from equation (21). We check this against the target value of ξ , and numerically adjust γ_4

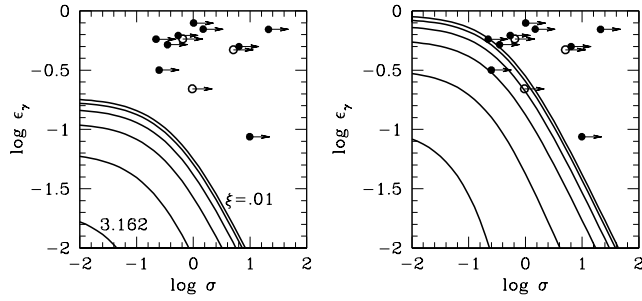


Figure 2. Similar to Fig. 1, but for a magnetized reverse shock. The curves correspond to jet Lorentz factor $\gamma_j = 300$ as measured in the lab frame, and (from below) relativity parameter $\xi = 3.162, 1, 0.3162, 0.1, 0.03162, 0.01$. The panel on the left is for $\epsilon_e = 0.2$ and that on the right for $\epsilon_e = 1$.

until we achieve the value of ξ we seek. At this point, we have the solution to the problem.

Once we have the solution, we can calculate the parameter ϵ_γ . As before, we will assume that a fraction ϵ_e of the gas thermal enthalpy in region 3 is radiated. As measured in the lab frame, this corresponds to an energy per particle of $\epsilon_e \gamma_c h(\theta_3) \theta_3 mc^2$. To calculate the total energy per particle of the system, it is simplest to consider the unshocked jet fluid. In its own rest frame, the enthalpy per particle is $mc^2(1 + \sigma)$, and this gets multiplied by γ_j when we transform to the lab frame.³ Thus we obtain

$$\epsilon_\gamma = \frac{\epsilon_e \gamma_c h(\theta_3) \theta_3}{\gamma_j (1 + \sigma)}. \quad (25)$$

Apart from ϵ_e , this reverse shock model has three parameters: the jet Lorentz factor γ_j , the magnetization parameter of the jet material σ , and the relativity parameter ξ . Figure 2 shows results for a fixed value of $\gamma_j = 300$ (the results hardly change for other values, e.g., 100 or 1000). The curves correspond to selected values of the relativity parameter ξ . As in the case of unmagnetized reverse shocks (SP95, Giannios et al. 2008), we find that the γ -ray efficiency is highest for highly relativistic shocks ($\xi \ll 1$), and the efficiency is very poor for Newtonian shocks ($\xi > 1$). In addition, for a given value of ξ , the efficiency decreases as the magnetization increases. This result is in qualitative agreement with the work of Zhang & Kobayashi (2005), Lyutikov (2005) and Giannios et al. (2008).

4.2 Comparison with GRB Data

As in the case of the internal shock model, a comparison of the predictions of the magnetized reverse shock model with GRB data (Fig. 2) indicates that the model has no hope of satisfying the observations. For $\epsilon_e = 0.2$, which we consider a reasonable value, not a single GRB agrees with the model even if we assume an extremely relativistic shock with $\xi = 0.01$. For $\epsilon_e = 1$, which in our opinion is rather optimistic, a few systems do fall inside the model curves, but far too many systems still remain unexplained. We thus conclude that, if jet ejections are cold and magnetized and are described by ideal MHD, then the magnetized reverse shock model considered here is ruled out by the data.

³ Note that, for both of the above quantities, we first calculate the enthalpy in the rest frame of the gas, where there is no net momentum. Thus, transformation of the energy to another frame requires only multiplication by the relevant Lorentz factor.

5 SUMMARY AND DISCUSSION

The magnetic acceleration paradigm for relativistic jets is theoretically appealing and widely accepted (Blandford 1976; Lovelace 1976; Begelman & Li 1994; Bogovalov 1997; Lyubarsky & Kirk 2001; Vlahakis & Königl 2003; see Beskin 2009 for a complete reference list). Recent advances in numerical techniques, coupled with analytical methods, have led to a deeper understanding of how Poynting-dominated jets accelerate to large Lorentz factors (Komissarov 2004; Komissarov et al. 2007, 2009, 2010; Tchekhovskoy et al. 2008, 2009, 2010a,b). In the specific context of ultra-relativistic GRB jets, it has recently been shown that the collimation angle θ_j and the Lorentz factor γ_j of a magnetically accelerated jet are not independent but are related via the magnetization parameter σ (Tchekhovskoy et al. 2010b). Estimates of θ_j and γ_j of GRB jets, obtained by modeling afterglow data, are generally consistent with these jets having $\sigma \sim 1$ just prior to the onset of the afterglow (Tchekhovskoy et al. 2010b). This indicates that GRB jets successfully convert about half of their initial Poynting flux to matter kinetic energy by the time they reach the deceleration radius. These jets are thus energetically efficient.

When it comes to radiative efficiency, however, $\sigma \sim 1$ is not sufficient. KC84 showed that perpendicular shocks in cold magnetized gas produce thermal energy very inefficiently unless σ is much less than unity. We have explored this issue in detail in the context of GRB internal shocks and reverse shocks. Both of these shocks occur in the material ejected in a GRB and are expected to be magnetized. The geometry is also such that the shocks will be perpendicular, i.e., the magnetic field will be perpendicular to the velocity vector, or parallel to the shock front. We have analyzed such shocks, assuming that a fraction ϵ_e of the gas thermal energy in the shocked gas goes into electrons and that this energy is entirely radiated in prompt radiation. We consider two values of ϵ_e , viz., $\epsilon_e = 0.2$, which we consider to be a reasonable estimate, and $\epsilon_e = 1$, which is highly optimistic.

Our calculations indicate that, once σ exceeds about 0.1, the efficiency of thermalization begins to fall noticeably, and that the drop becomes quite precipitous once $\sigma > 1$ (Figs. 1, 2). GRB observations indicate that the prompt γ -ray emission is quite efficient, with the efficiency parameter ϵ_γ (defined in eq. 12) being typically of order 0.5 or larger (Table 1). On the other hand, not a single GRB has $\sigma < 0.1$, as needed to obtain such high efficiency in a cold magnetized shock, and half our sample has $\sigma > 1$, where radiative efficiency is very poor. The implication is that GRB prompt emission cannot be produced by either internal shocks or the reverse shock, if jets are cold and magnetically accelerated. This conclusion is hard to avoid. Even with very optimistic assumptions, e.g., all the thermal energy goes into electrons ($\epsilon_e = 1$, which might happen if the jet is made entirely of electrons and positrons), and is immediately radiated in γ -rays, the calculated efficiency is far below what is needed to explain the observations.

We consider here several possible resolutions of this puzzle, none of which is very satisfactory.⁴

One possibility is to associate the prompt emission with the forward shock, which is very weakly magnetized ($\sigma \ll 1$) and therefore converts a large fraction of the jet kinetic energy into thermal energy. This alone is not enough since the thermal energy must

⁴ Zhang & Yan (2011) have considered internal collisions for a magnetically dominated outflow and suggest that this could facilitate dissipation of magnetic energy via reconnection. We do not discuss this particular process here.

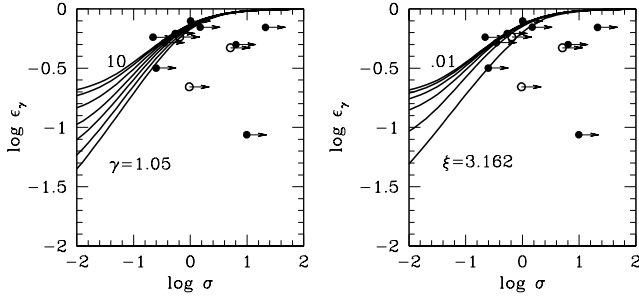


Figure 3. Similar to Figs. 1 and 2, except it is assumed that, in addition to a fraction $\epsilon_e = 0.2$ of the gas thermal enthalpy, the entire magnetic enthalpy is also radiated as prompt γ -rays. The panel on the left is for an internal shock and that on the right for a reverse shock.

then be radiated with greater than 50% efficiency in order to explain the observed values of ϵ_γ . Therefore, nearly all the thermal energy should go into electrons ($\epsilon_e \sim 1$), which is very unlikely for the electron-proton plasma we expect to be present in the forward shock. In any case, the forward shock has been convincingly associated with afterglow emission (Gehrels et al. 2009; Meszaros 2002; Piran 2005; Zhang 2007; and references therein), and it does not seem likely that the same region will also produce the prompt emission.

A second possibility is that much of the magnetic energy in a GRB shock is somehow converted to particle thermal energy. That is, when σ is large and most of the energy density in the post-shock gas is in the form of magnetic energy, there is a mechanism whereby this energy is converted to particle energy. A scenario where this can happen is if the pre-shock gas is “striped” as in current models of energy dissipation in the magnetized wind of pulsars (Lyubarsky & Kirk 2001; Lyubarsky 2010a). A striped morphology is not obvious for a GRB jet (but see McKinney & Uzdensky 2010). However, if it is present, we do expect a substantial fraction of the magnetic energy to be dissipated in the shock. Figure 3 shows results for a hypothetical model in which we assume that, in addition to a fraction $\epsilon_e = 0.2$ of the gas thermal enthalpy, 100% of the magnetic energy is radiated. This model does explain the GRB observations but at the price of making a very extreme (and theoretically unsupported) assumption. We do not endorse this model but present it merely as a way to emphasize how difficult it is to explain the radiative efficiency of GRB prompt emission.

A third possibility is that the magnetic energy is dissipated, not through a shock, but through some other “current-driven” mechanism such as reconnection. Poynting-dominated magnetically accelerated jets are fairly stable once they are ultra-relativistic (e.g., Narayan, Li & Tchekhovskoy 2009) and are unlikely to have large-amplitude fluctuations that might drive reconnection. However, it is conceivable that these jets lose their stability once they reach a large radius (McKinney & Uzdensky 2010), e.g., the deceleration radius where the jet meets the external medium and begins to slow down. Whether the instability would be powerful enough to drive wholesale reconnection and convert most of the magnetic energy into particle energy is an open question. As Fig. 3 shows, something like this is needed if one is to explain the data.

Another possibility is that our assumption of cold gas, whose acceleration is entirely by magnetic means, is incorrect. Non-relativistic MHD simulations of magnetized jets (Moll, Spruit & Obergaulinger 2008; Moll 2009) indicate that these jets develop a kink instability which might lead to dissipation. We could then have a scenario in which the jet starts off mag-

netically dominated at the base but quickly dissipates its magnetic energy into heat while the jet is still non- or quasi-relativistic. Further acceleration of the jet is then driven by the thermal pressure of the heated gas. Thus, we no longer have a magnetically driven jet, but something akin to the standard fireball model of a GRB. Clearly, the calculations presented here, which are restricted to cold magnetized gas, are not relevant for such a model.

Finally, it is possible that the prompt emission in GRBs is not produced in the jet at a large distance from the progenitor, but rather in the photospheric region where the jet ejecta first become transparent. Models of this form have been developed (Thompson 1994; Meszaros & Rees 2000; Rees & Meszaros 2005; Pe’er, Meszaros, Rees 2006; Giannios 2008; Beloborodov 2010; Metzger et al. 2011) and it is claimed that they produce prompt γ -ray emission with high radiative efficiency and with the correct spectrum (e.g., Pe’er & Ryde 2011; Uzdensky, Beloborodov & Poutanen 2011). Magnetic fields may play a role in photospheric models (Uzdensky & McKinney 2010), but the role of shocks is unclear. Our analysis is not applicable to these models.

ACKNOWLEDGMENTS

RN and AT were supported in part by NASA grant NNX11AE16G and NSF grant AST-1041590, and by NSF through TeraGrid resources provided by QueenBee of the Louisiana Optical Network Initiative (<http://www.loni.org>) and Kraken of the National Institute for Computational Sciences (<http://www.nics.tennessee.edu>) under grant number TG-AST080026N (RN & AT) and TG-AST100040 (AT). AT was supported in part by a Princeton Center for Theoretical Science Fellowship. PK was supported in part by NSF grant AST-0909110.

APPENDIX A: ANALYTICAL APPROXIMATIONS FOR A PERPENDICULAR SHOCK

A cold hydrodynamic flow can have a shock for any choice of the upstream velocity u_u . This is because no signals can propagate in the cold gas and so the upstream gas is always supersonic. A magnetized fluid is different. Even if the gas is cold, Alfvén and fast magnetosonic waves can still propagate in the fluid. Thus a shock is possible only if the upstream gas moves faster than these waves.

For the particular geometry we have considered, viz., a perpendicular shock with magnetic field perpendicular to the velocity vector, the relevant wave speed is that of the fast magnetosonic wave, which is given (in the comoving frame of the gas) by

$$\beta_{\text{fms}}^2 = \frac{\sigma}{\sigma + 1}, \quad u_{\text{fms}}^2 = \sigma. \quad (\text{A1})$$

Thus we can have a shock only if

$$u_u^2 > \sigma. \quad (\text{A2})$$

We now consider a number of limiting cases. When $u_u^2 \gg \sigma$, we expect to have a strong shock, whereas when u_u^2 is only marginally greater than σ , we expect a weak shock. In addition, we have different results depending on whether $u_u^2 \gg 1$ (ultrarelativistic) or $u_u^2 \ll 1$ (nonrelativistic), and on whether $\sigma \gg 1$ (strongly magnetized) or $\sigma \ll 1$ (weakly magnetized). KC84 considered a couple of important cases, but here we present scalings for all the different regimes. Figure A1 identifies the regimes and labels them by the respective subsection where each is discussed.

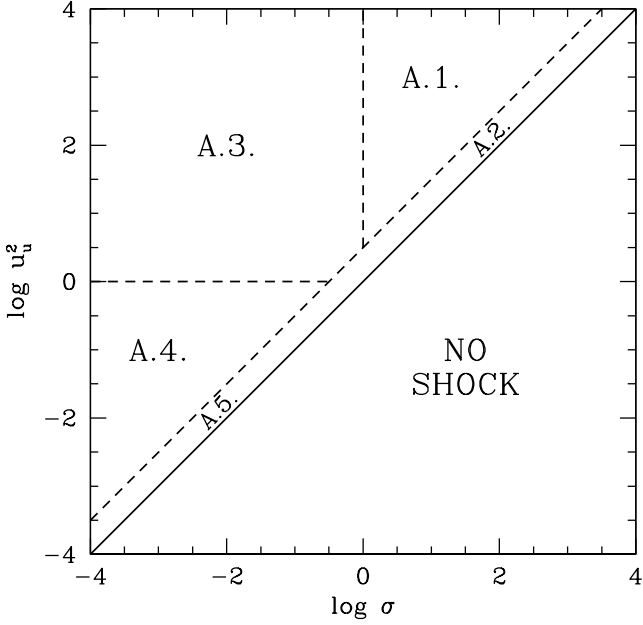


Figure A1. Shows different regimes for a perpendicular shock in cold upstream gas. The horizontal axis indicates the magnetization parameter σ of the upstream gas (eq. 2) and the vertical axis indicates the square of the upstream relativistic velocity u_u as measured in the frame of the shock. There is no shock when $u_u < \sqrt{\sigma}$ since the upstream gas moves slower than the fast magnetosonic wave speed $u_{fms} = \sqrt{\sigma}$ (eqs. A1, A2). The regions marked A.1, ..., A.5, in the plot correspond to different shock regimes. The labels refer to the section numbers in Appendix A where each is discussed. Regions A.1. and A.2. correspond to highly magnetized shocks ($\sigma \gg 1$), which are necessarily also highly relativistic ($u_u \gg 1$). A.1. describes a strong shock, where $u_u \gg \sqrt{\sigma}$, while A.2. describes a weak shock where u_u is only marginally greater than $\sqrt{\sigma}$. Regions A.3., A.4., A.5., correspond to weakly magnetized shocks ($\sigma \ll 1$). A.3. is highly relativistic ($u_u \gg 1$), where the shock is necessarily strong. A.4. is non-relativistic ($u_u \ll 1$), but still with a strong shock, while A.5. corresponds to a non-relativistic weak shock, where u_u is only marginally greater than $\sqrt{\sigma}$.

A1 Strong Relativistic Shock with Strong Magnetization:

$$u_u^2 \gg \sigma \gg 1$$

This case has been considered by KC84 who give the following results:

$$u_d^2 \approx \sigma + \frac{1}{8} + \frac{1}{64\sigma} + o\left(\frac{1}{\sigma}\right), \quad (\text{A3})$$

$$\frac{B_d}{B_u} \approx 1 + \frac{1}{2\sigma} - \frac{3}{16\sigma^2} + o\left(\frac{1}{\sigma^2}\right), \quad (\text{A4})$$

$$\frac{\theta_d}{u_u} \approx \frac{1}{8\sqrt{\sigma}} \left(1 - \frac{3}{16\sigma}\right) + o\left(\frac{1}{\sigma^{3/2}}\right), \quad (\text{A5})$$

where $o(x)$ denotes terms of higher order than x , i.e., $o(x)/x \rightarrow 0$ as $x \rightarrow 0$. In the above, we remind the reader that the magnetic field strengths B_u and B_d are measured in the shock frame. These results are obtained by expanding the jump conditions as power series in the small quantity $1/\sigma$, and matching terms of similar order. We have set $h(\theta_d) = 4$, as appropriate for relativistically hot downstream gas. Our result for θ_d/u_u differs from that given in KC84.

A2 Weak Relativistic Shock with Strong Magnetization:

$$u_u^2 \rightarrow \sigma \gg 1$$

As u_u^2 approaches σ , the shock becomes progressively weaker. Let us write $u_u^2 = \sigma(1 + \Delta)$, with $\Delta \ll 1$. As Δ becomes progressively smaller, less and less of the kinetic energy of the upstream gas is thermalized in the shock. In this limit, the downstream temperature θ_d becomes non-relativistic and so we set $h(\theta_d) = 5/2$. In this limit, the leading terms in the solution are as follows:

$$u_d^2 \approx \sigma \left[1 - \frac{\Delta}{3} + \frac{44}{81} \left(1 - \frac{3}{11\sigma}\right) \Delta^2 \right] + o(\Delta^2), \quad (\text{A6})$$

$$\frac{B_d}{B_u} \approx 1 + \frac{2}{3\sigma} \left(1 - \frac{1}{\sigma}\right) \Delta - \frac{58}{81\sigma} \Delta^2 + o\left(\frac{\Delta^2}{\sigma}; \frac{\Delta}{\sigma^2}\right), \quad (\text{A7})$$

$$\theta_d \approx \frac{4}{81} \left(1 - \frac{1}{\sigma} + \frac{1}{\sigma^2}\right) \Delta^3 - \frac{8}{81} \left(1 - \frac{4}{3\sigma}\right) \Delta^4 + o\left(\frac{\Delta^3}{\sigma^2}; \frac{\Delta^4}{\sigma}\right). \quad (\text{A8})$$

Note that the leading term in the temperature of the shocked gas goes as Δ^3 , i.e., the shock is extremely inefficient. This is a characteristic feature of weak shocks.

A3 Strong Relativistic Shock with Weak Magnetization:

$$u_u^2 \gg 1 \gg \sigma$$

This case has again been considered by KC84. With $h(\theta_d) = 4$, the results are

$$u_d^2 \approx \frac{1}{8} + \frac{9}{8}\sigma - \frac{9}{8}\sigma^2 + o(\sigma^2), \quad (\text{A9})$$

$$\frac{B_d}{B_u} \approx 3 - 12\sigma + 96\sigma^2 + o(\sigma^2), \quad (\text{A10})$$

$$\frac{\theta_d}{u_u} \approx \frac{1}{3\sqrt{2}} \left(1 - \frac{5}{2}\sigma + \frac{111}{8}\sigma^2\right) + o(\sigma^2). \quad (\text{A11})$$

Again, our result for θ_d differs from that given in KC84. The results for an unmagnetized relativistic shock are recovered by simply setting $\sigma = 0$ in the above relations.

A4 Strong Non-Relativistic Shock with Weak Magnetization:

$$1 \gg \beta_u^2 \gg \sigma$$

Here we consider the non-relativistic case and replace u_u , u_d by β_u , β_d . Also, we set $h(\theta_d) = 5/2$. Then we find

$$\beta_d \approx \frac{1}{4}\beta_u + \frac{9}{8}\frac{\sigma}{\beta_u} - \frac{9}{4}\frac{\sigma^2}{\beta_u^3} + o\left(\frac{\sigma^2}{\beta_u^3}\right), \quad (\text{A12})$$

$$\frac{B_d}{B_u} \approx 4 - 18\frac{\sigma}{\beta_u^2} + 117\frac{\sigma^2}{\beta_u^4} + o\left(\frac{\sigma^2}{\beta_u^4}\right), \quad (\text{A13})$$

$$\theta_d \approx \frac{3}{16}\beta_u^2 - \frac{21}{16}\sigma + o(\sigma). \quad (\text{A14})$$

The solution for an unmagnetized shock is obtained by setting $\sigma = 0$. As an aside, we note that σ is related to the Alfvén wave speed v_A by

$$\sigma = \frac{B^2}{4\pi n m c^2} = \frac{v_A^2}{c^2} = \beta_A^2. \quad (\text{A15})$$

A5 Weak Non-Relativistic Shock with Weak Magnetization:

$$1 \gg \beta_u^2 \rightarrow \sigma$$

Finally, we consider the case when the shock is non-relativistic and $\beta_u = \sqrt{\sigma}(1 + \Delta)$ with $\sqrt{\sigma} \ll \Delta \ll 1$. In this limit, we find

$$\beta_d \approx \left(1 - \frac{1}{3}\Delta + \frac{46}{81}\Delta^2\right) \sqrt{\sigma} + o(\Delta^2 \sqrt{\sigma}), \quad (\text{A16})$$

$$\frac{B_d}{B_u} \approx 1 + \frac{4}{3}\Delta - \frac{10}{81}\Delta^2 + o(\Delta^2), \quad (\text{A17})$$

$$\theta_d \approx \left(\frac{32}{81}\Delta^3 - \frac{112}{243}\Delta^4\right) \sigma + o(\Delta^4 \sigma). \quad (\text{A18})$$

APPENDIX B: THE RELATIVITY PARAMETER ξ

We generalize the discussion of the parameter ξ given in SP95, following the analysis of Giannios et al. (2008). We consider a spherically expanding shell of cold magnetized jet material of radius R , shell thickness Δ , and Lorentz factor γ_j , all measured in the lab frame. The ‘‘spreading radius’’ of the shell is given by

$$R_s = \gamma_j^2 \Delta. \quad (\text{B1})$$

The total (isotropic equivalent) energy of the shell is

$$E = 4\pi R^2 \Delta n_4 m c^2 \gamma_j^2 (1 + \sigma) \equiv M_{\text{ej}} \gamma_j c^2 (1 + \sigma), \quad (\text{B2})$$

where n_4 is the rest frame particle number density of the jet material, σ is the magnetization of the material, and M_{ej} is the total rest mass of the shell. From E , we obtain the ‘‘Sedov length’’ ℓ and the ‘‘deceleration radius’’ R_{dec} ,

$$\ell = \left(\frac{3E}{4\pi n_1 m c^2}\right)^{1/3} = \left[\frac{3M_{\text{ej}} \gamma_j (1 + \sigma)}{4\pi n_1 m}\right]^{1/3}, \quad (\text{B3})$$

$$R_{\text{dec}} = \frac{\ell}{\gamma_j^{2/3}} = \left[\frac{3M_{\text{ej}} (1 + \sigma)}{4\pi n_1 m \gamma_j}\right]^{1/3}, \quad (\text{B4})$$

where n_1 is the number density of the external ambient medium. Substituting for M_{ej} (with $R = R_{\text{dec}}$) in the equation for R_{dec} , we find that

$$R_{\text{dec}} = 3\Delta \frac{n_4}{n_1} (1 + \sigma), \quad (\text{B5})$$

from which we obtain

$$\xi = \left(\frac{R_{\text{dec}}}{R_s}\right)^{1/2} = \left[\frac{3}{\gamma_j^2} \frac{n_4}{n_1} (1 + \sigma)\right]^{1/2}. \quad (\text{B6})$$

Note that n_4 is the number density of the jet ejecta at the moment when the shell radius R is equal to R_{dec} .

REFERENCES

- Abdo, A.A., et al. 2009, *Sci.*, 323, 1688
 Ackermann, M., et al. 2010, *ApJ*, 716, 1178
 Begelman, M.C. & Li, Zh-Yu 1994, *ApJ* 426, 269
 Beloborodov, A.M. 2010, *MNRAS* 407, 1033
 Beskin, V. S. 2009, *MHD Flows in Compact astrophysical Objects: Accretion, Winds and Jets*, Springer
 Blandford, R.D. 1976, *MNRAS* 176, 465
 Bloom, J., Frail, D., Kulkarni, S.R. 2003, *ApJ*, 594, 674
 Bogovalov, S.V. 1997, *AA* 327, 662
 Chandrasekhar, S. 1960, *Radiative Transfer*, Dover: New York
 Gehrels, N., Ramirez-Ruiz, E., Fox, D.B., 2009, *Ann. Rev. A&A* 47, 567
 Giannios, D. 2008, *A&A*, 480, 305

- Giannios, D., Mimica, P., Aloy, M. A. 2008, *A&A*, 478, 747
 Greiner, J., et al. 2009, *A&A*, 498, 89
 Kennel, C. F., Coroniti, F. V. 1984, *ApJ*, 283, 694 (KC84)
 Komissarov, S.S. 2004, *MNRAS* 350, 1431
 Komissarov, S.S., Barkov, M., Vlahakis, N., Königl, A. 2007, *MNRAS* 380, 51
 Komissarov, S. S., Vlahakis, N., Königl, A., & Barkov, M. V. 2009, *MNRAS*, 394, 1182
 Komissarov, S. S., Vlahakis, N., Königl, A. 2010, *MNRAS*, 407, 17
 Kumar, P. 1999, *ApJ*, 523, L113
 Kumar, P., Barniol Duran, R. 2009, *MNRAS*, 400, L75
 Kumar, P., Barniol Duran, R. 2010, *MNRAS*, 409, 226
 Lazar, A., Nakar, E., Piran, T. 2009, *ApJ*, 695, L10
 Lazzati, D., Ghisellini, G., Celotti, A. 1999, *MNRAS* 309, L13
 Li, Z.-Y., Chevalier, R. A. 2003, *ApJ*, 589, L69
 Lovelace, R.V.E. 1976, *Nature*, 262, 649
 Lyubarsky, Y. 2010a, *ApJ* 725, 234
 Lyubarsky, Y. E. 2010b, *MNRAS*, 402, 353
 Lyubarsky, Y., Kirk, J.G. 2001, *ApJ* 547, 437
 Lyutikov, M. 2005, preprint (arXiv:astro-ph/0503505)
 Uzdensky, D. A., McKinney, J. C. 2011, *Physics of Plasmas*, 18, 042105
 McKinney J., Uzdensky D., 2010, preprint (arXiv:1011.1904)
 Meszaros, P., 2002, *Ann. Rev. A&A* 40, 137
 Meszaros, P., Rees, M.J. 2000, *ApJ* 530, 292
 Metzger, B. D., Giannios, D., Thompson, T. A., Bucciantini, N., & Quataert, E. 2011, *MNRAS*, 413, 2031
 Moll, R. 2009, *A&A*, 507, 1203
 Moll, R., Spruit, H. C., Obergaulinger, M. 2008, *A&A*, 492, 621
 Narayan, R., Kumar, P. 2009, *MNRAS*, 394, L117
 Narayan, R., Li, J., Tchekhovskoy, A. 2009, *ApJ*, 697, 1681
 Narayan, R., Paczynski, B., Piran, T., 1992, *ApJ*, 395, L83
 Panaitescu, A., Kumar, P. 2002, *ApJ*, 571, 779 (PK02)
 Panaitescu, A., Spada, M., Meszaros, P. 1999, *ApJ*, 522, L105
 Pe’er, A., Meszaros, P., Rees, M.J. 2006, *ApJ* 652, 482
 Pe’er, A., Ryde, F. 2011, *ApJ*, 732, 49
 Piran, T., 2005, *Reviews of Modern Physics*, 76, 1143
 Rees, M.J., Meszaros, P. 2005, *ApJ* 628, 847
 Rees, M.J., Meszaros, P., 1994, *ApJ*, 430, L93
 Sari, R., Piran, T. 1995, *ApJ*, 455, L143 (SP95)
 Sari, R., Piran, T. 1997, *ApJ*, 485, 270
 Service, A. T. 1986, *ApJ*, 307, 60
 Tchekhovskoy, A., McKinney, J. C., & Narayan, R. 2008, *MNRAS*, 388, 551
 Tchekhovskoy, A., McKinney, J. C., Narayan, R. 2009, *ApJ* 699, 1789
 Tchekhovskoy, A., Narayan, R., & McKinney, J. C. 2010a, *ApJ*, 711, 50
 Tchekhovskoy, A., Narayan, R., McKinney, J. C. 2010b, *New Astron.*, 15, 749
 Thompson, C. 1994, *MNRAS* 270, 480
 Vlahakis, N., Königl, A. 2003, *ApJ* 596, 1080
 Vurm, I., Beloborodov, A. M., Poutanen, J. 2011, arXiv:1104.0394
 Woosley, S.E., Bloom, J.S. 2006, *Ann. Rev. A&A*, 44, 507
 Zhang, B. 2007, *Chinese Journal of Astronomy and Astrophysics*, 7, 1
 Zhang, B., Yan, H. 2011, *ApJ* 726, 90
 Zhang, B., Kobayashi, S. 2005, *ApJ*, 628, 315